Available online at www.sciencedirect.com

ScienceDirect

Procedia CIRP 71 (2018) 329–334

www.elsevier.com/locate/procedia

4th CIRP Conference on Surface Integrity (CSI 2018)

Prediction of residual stress in precision milling of AISI H13 steel

Andreas Reimer[ab], Xichun Luo[a]*

[a]University of Strathclyde, Centre for Precision Engineering, 75 Montrose St, Glasgow G1 1XJ, United Kingdom
[b]Advanced Forming Research Centre, 85 Inchinnan Dr, Inchinnan, Renfrew PA4 9LJ, United Kingdom

* Corresponding author. *Tel.*: +441415745280. *E-mail address*: xichun.luo@strath.ac.uk

Abstract

Surface integrity describes the attributes of a surface and it influences the functional performance of a work piece significantly. Residual stress is one of the major characterization parameters of surface integrity. Non-favorable residual stresses on a machined surface can reduce the fatigue life and performance of the machined part. It therefore requires a prediction model for residual stress in order to establish machining strategy to obtain favorable residual stress for prolonged fatigue life. Hardened tool steels have been widely used to make molds and dies by precision milling in aerospace and automotive industries. Knowledge of the relationship between residual stress on the machined molds and machining conditions is very important for process control. In this work, a prediction model for residual stress was developed by using a model-based approach on an Artificial Neural Network. This model is expected to predict the residual stress based on cutting parameters such as cutting speed, feed rate, depth of cut and tool lead angle. Several precision milling trials were carried out using a central composite design method. The networks have been trained and validated by experimental results. The performance of a feed forward neural network model with backpropagation was assessed and compared with a radial basis function network model by criterion of least mean squared error. Furthermore, the neural network prediction model was supported by the finite element simulation of the milling process to understand the formation mechanism of the residual stress in the machined surface. It was found, that the predicted values by the neural network model matched well with the experimental results. The radial basis function network showed better results than the feed forward network and was therefore chosen to take forward in the analysis. The feed rate was in this case the most influential factor, because it contributes significantly to heat and deformation on the work piece. The model could be used to optimize machining processes to obtain machining strategy for generating favorable residual stress and increasing fatigue life performance of the machined parts.

Selection and peer-review under responsibility of the scientific committee of the 4th CIRP Conference on Surface Integrity (CSI 2018).

Keywords: Residual Stress prediction; artificial neural network; tool steel; HSM

1. Introduction

Surface integrity describes the attributes of a surface and it influences the functional performance of a work piece significantly. Residual stress is one of the major characterization parameters of surface integrity. Previous studies have shown, that residual stress can have a significant influence on the fatigue life / performance and distortion of the work piece [1-5]. High speed precision machining processes have been used in automotive, aerospace and tooling industries over the last few decades. To improve a part surface quality in particular the surface integrity and increasing product life cycle are important aspects for these manufacturing industries [1-4]. Hard material, namely tools steel such as AISI D2 and H13, are very commonly used as dies or molds for forming and forging processes. Nowadays these dies and molds require high precision to allow industries such as automotive and aerospace to build near net-shape forms. Therefore, it is important to build a knowledge bridge between residual stress and the machining process, to increase the performance of those forging / forming dies and to ultimately achieve higher accuracy and reduce manufacturing costs. This is the reason why this area is still being researched, especially to understand and predict residual stresses, which occur during the machining process and remain in the work piece.

This paper will investigate the formation and influential factors of residual stress during high speed machining process

Selection and peer-review under responsibility of the scientific committee of the 4th CIRP Conference on Surface Integrity (CSI 2018).
10.1016/j.procir.2018.05.036

using a ball nose end mill cutter. This includes extensive set of machining trials based on a central composite design method with four factors, namely, cutting speed, feed rate, depth of cut and tool lead angle. The results were analyzed and used to develop artificial neural networks models for the prediction of residual stress. Two different types of artificial neural network models were assessed and compared based on their mean squared error performance and regression accuracy. Conclusions were drawn based on these analyses.

2. Experiments

Table 1. Experimental design

Standard Order	Cutting speed (m/min)	Depth of Cut (mm)	Feed Rate (mm/tooth)	Lead Angle (deg)
1	350	0.3	0.08	7.5
2	250	0.5	0.08	7.5
3	250	0.3	0.16	7.5
4	350	0.5	0.16	7.5
5	250	0.3	0.08	22.5
6	350	0.5	0.08	22.5
7	350	0.3	0.16	22.5
8	250	0.5	0.16	22.5
9	300	0.4	0.12	15
10	300	0.4	0.12	15
11	250	0.3	0.08	7.5
12	350	0.5	0.08	7.5
13	350	0.3	0.16	7.5
14	250	0.5	0.16	7.5
15	350	0.3	0.08	22.5
16	250	0.5	0.08	22.5
17	250	0.3	0.16	22.5
18	350	0.5	0.16	22.5
19	300	0.4	0.12	15
20	300	0.4	0.12	15
21	200	0.4	0.12	15
22	400	0.4	0.12	15
23	300	0.1	0.12	15
24	300	0.6	0.12	15
25	300	0.4	0.02	15
26	300	0.4	0.2	15
27	300	0.4	0.12	0
28	300	0.4	0.12	45
29	300	0.4	0.12	15
30	300	0.4	0.12	15

The machining experiments were conducted on a DMG Mori-Seki HSC 75 with a tungsten carbide 4 flute ball nose end milling cutter of 8 mm diameter (Mitsubishi - impact miracle). The cutting speed of 200 – 400 m/min, depth of cut of 0.1 – 0.6 mm, feed rate of 0.02 – 0.2 mm/tooth with tool lead angle of 0 – 45 deg were adopted in the experiments. AISI H13 tool steels with an average hardness of 49 HRC were used as work materials.

The experiments were planned based on a 5-level Central Composite Design (CCD) method which led to a total of 30 samples where the run-order was randomized. The experimental design can be found in Table 1. 7 additional experiments were also carried out for validation of the developed neural network prediction models.

The experimental setup is shown in Fig. 1. The work piece is fixed on a fixture (as shown in Fig. 1 (b) which is mounted on top of a Kistler dynamometer (Type 9129AA) for measuring the cutting forces. Fig. 1 (c) shows the laptop computer and signal conditioner to process the cutting force data.

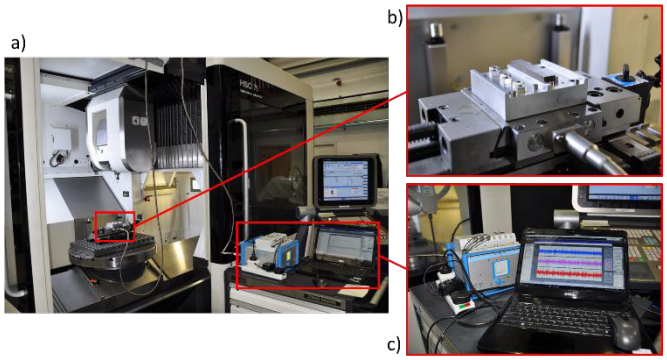

Fig. 1. Experimental setup, (a): complete machine setup; (b): work piece with its holder and dynamometer; (c): Cutting force data processing equipment.

Table 2. Experimental Von-Mises results

Standard Order	Von-Mises (MPa)	Standard Order	Von-Mises (MPa)
1	165.74	16	181.52
2	113.74	17	119.37
3	103.04	18	159.77
4	115.29	19	181.39
5	158.42	20	113.02
6	147.961	21	121.45
7	150.58	22	145.88
8	109.34	23	133.67
9	130.19	24	146.97
10	114.23	25	173.96
11	130.71	26	208.02
12	113.21	27	198.11
13	108.16	28	161.02
14	125.96	29	120.46
15	159.22	30	153.30

A Proto LXRD with a Chromium (Cr) tube and a Bragg-angle of 156.4° (2θ) was used to measure the residual stress. Each sampling point was measured in 5 different angles in the longitudinal and perpendicular directions to the cutting direction. Furthermore, each work piece sample was measured 5 times to calculate an average. The measurement of two perpendicular stress vectors and shear stress in one point

allows the calculation of the Von-Mises plane stress (VM). Table 2 shows the calculated Von-Mises plane stresses for each sample which were used to assess the correlation between the FEM simulation and XRD measurement.

3. Finite Element Simulation Setup

In order to gain fundamental understanding of the physics of formation of residual stress finite element (FE) simulation of machining process was also carried out in this paper,. Fig. 2 shows the FE simulation model established in ABAQUS 6-14. The cutting tool was 3D-scanned prior FE implementation to increase accuracy of the simulation. It was modelled with rigid shell elements to reduce the calculation time. The work piece has 8-node thermally coupled brick, trilinear displacement and temperature, reduced integration and hourglass control elements (C3D8RT). The element deletion in the work piece elements was activated.

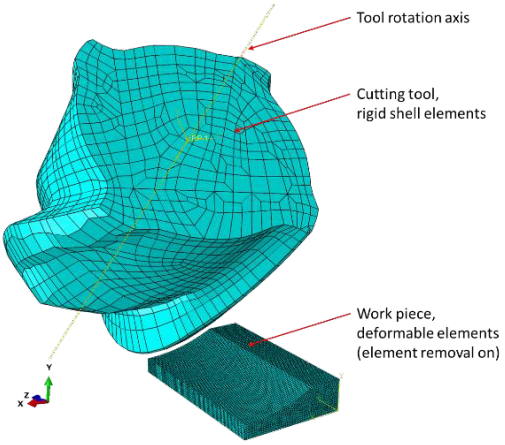

Fig. 2. FEM setup

The model can be used to analyze cutting temperature, residual stress, cutting forces etc. during the cutting process with multi-flute engagement. Therefore, the precision of this calculated model is vital to reflect accurate predictions.

This FE model used the extended Johnson-Cook model (JC) (equation 1) as well as an additional material removal subroutine [6, 7]. This subroutine deletes elements, which exceed the ultimate tensile strength (UTS) and which is varying depending on the temperature. The temperature change in the material effects the UTS and therefore the material removal criteria, it is commonly known that the UTS decreases with increasing temperatures [8], based on this the subroutine adjusts the UTS. Due to this additional criterion, a higher accuracy of simulation can be achieved. The criterion is an empirical 3rd degree regression formula based on temperature variating tensile experiments, the principal can be found in [7].

$$\bar{\sigma}\left(\bar{\varepsilon},\dot{\bar{\varepsilon}},T\right)=\left(A+B\left(\bar{\varepsilon}\right)+D\ln\left(\varepsilon_0+\varepsilon\right)+E\right)\cdot \left(1+C\ln\frac{\dot{\bar{\varepsilon}}}{\dot{\bar{\varepsilon}}_0}\right)\cdot\left(1-\left(\frac{T-T_0}{T_m-T_0}\right)^m\right) \quad (1)$$

In equation 1, the flow stress $\bar{\sigma}$ can be combined by the Von-Mises yield criterion and describes an isotropic hardening, where $\bar{\varepsilon}$ is the proportional strain, $\dot{\bar{\varepsilon}}$ is the proportional strain rate and T is the temperature. A, B, C, m, n, T_0, T_m are material parameters in the Johnson-Cook equation, ε_0 is the reference strain and ε the current strain. Parameter D and E are 2nd and 3rd grade polynomial regression, respectively. In the following table 3 the used parameter in the FE model can be found.

Table 3. Johnson-Cook material parameter for AISI H13

Hardness [HRC]	A [MPa]	B [MPa]	C [-]	n [-]	m [-]	T_m [°K]	Source
46	674.8	239.2	0.027	0.28	1.3	1760	[9]

4. Artificial Neural Network model

4.1. Artificial Neural Network Structure

In the recent years machine learning or artificial intelligence has gained ever more attentions in research. Therefore the prediction results can achieve a very high accuracy and can predict more complex problems compared to other prediction methods. Machine learning can be divided in several different methods; the most common methods are the artificial neural network, Fuzzy Logic, etc. Substantial literature has already been published in this area of research [5, 10-16].

The artificial neural network (ANN) imitates the human brain structure whereby it consists of an input layer, followed by a hidden layer of neurons and an output layer. The ANN can be further divided into different types of networks, like Feed Forward (FF), Radial Basis Function (RBF), Recurrent Neural Network, Dynamic Neural Networks, etc. [11, 14]. In this work the main focus is on the FF and RBF type of neural networks.

In general the FF network can have any number of hidden layers and any number of neurons in each layer of the hidden layers. Each neuron is constructed with an initial weight and every neuron is connected to each other from one layer to the other. The feed forward network usually needs to be trained, like a human brain, with each training cycle the network gains more knowledge and accuracy since the weights are re-adjusting accordingly to the target.

The Radial Basis Function has a similar structure as a FF network, however it only consists of one hidden layer and therefore the network has in most cases a simpler structure and works faster than a ‘traditional’ FF or multiplayer perceptron network (MLP). The RBF uses a classification by hyper spheres which is the biggest and most important difference from the FF network; the MLP networks using arbitrarily shaped hyper surfaces for its separation [10].

4.2. Artificial Neural Network Model Framework

In this work, two neural networks were used and the performance of both networks was compared based on its regression accuracy as well as the Mean Squared Error (MSE).

Matlab (R2017a) Toolbox Neural Network (Ver. 10.0) was used to realize the neural networks.

A sequential order of networks was tested with three hidden layers and neurons ranged between 1 to 10 in each layer, which result in 1000 tested networks. The training, validation and test ratio of those FF networks was 70:15:15, respectively. Fig. 3 shows the best structure of the FF network.

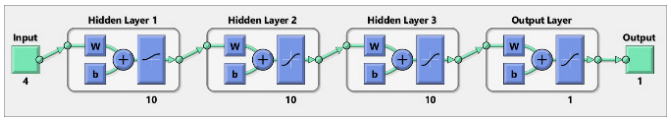

Fig. 3. FF Network structure

This network consists of an input layer, three hidden layers with each 10 neurons and an output layer. Every tested network has been trained 200 times to achieve consistent outcome. It was found that when the activation functions of the hidden layers were using a combination, it can increase the performance of the network. In this work, the best performance was achieved when the first hidden layer is set to a Log-Sigmoid activation function (equation 2); the following two hidden layers and the output layer to a hyperbolic-tangent sigmoid activation function (equation 3).

$$logsig(x) = \frac{1}{1+e^{-x_i}} \tag{2}$$

$$tansig(x) = \frac{e^{x_i} - e^{-x_i}}{e^{x_i} + e^{-x_i}} \tag{3}$$

The training of the neural network was based on the backpropagation function. The algorithm can be described in the following sequence; in the first step the input goes through the system and the MSE is calculated then, from the output the sensitivity is propagated back to the first layer and the weights, biases are updated [5].

The MSE is a function to measure and evaluate the performance in neural networks and can be defined as follows in equation 4:

$$MSE = \frac{1}{n}\sum_{k=1}^{n}(y_k - t_k)^2 \tag{4}$$

Where n indicates the number of total data patterns, y_k is the output generated by the neural network at point k and t_k is the target value at point k. To investigate the actual distance between the output and targets, the Root Mean Squared Error (RMSE) can be calculated as follows in equation 5:

$$RMSE = \sqrt{\frac{1}{n}\sum_{k=1}^{n}(y_k \quad t_k)^2} \tag{5}$$

Additionally from the more ‘traditional’ feed forward network with backpropagation (FFBP), the Radial Basis Function Network (RBF) is presented in the following paragraph. The general structure of the RBF, can be found in Fig. 4, the network also consists of an input layer, one hidden layer and an output layer. The hidden layer has 37 neurons (the same amount as the entire experiment).

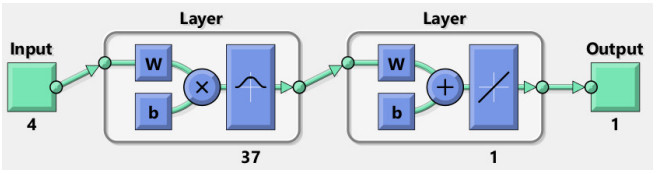

Fig. 4. RBF Network structure

The hidden layer uses a Gaussian activation function, see formula 6. Whereby x_i is weighted input vector for the specific neuron i; c_i is the center of neuron i and ω_i is the width of neuron i [10].

$$rbf(x) = e^{\left(-\frac{\|x_i - c_i\|^2}{\omega_i}\right)} \tag{6}$$

5. Results and Discussion

5.1. Neural Network results

In this work $\sin^2\psi$ method was used to calculate the residual stress in the AISI H13 work piece measured by the Proto LXRD with 30 kV voltage.

Fig. 5 shows the regression analysis results if the predicted residual stress by FFBP. This regression analysis consists of four components; training, validation, test and overall. This analysis shows that the overall status can achieve an accuracy of 81.71 %. The performance based on the MSE was calculated to 303.19 $(MPa)^2$, which means a RMSE of 17.41 MPa.

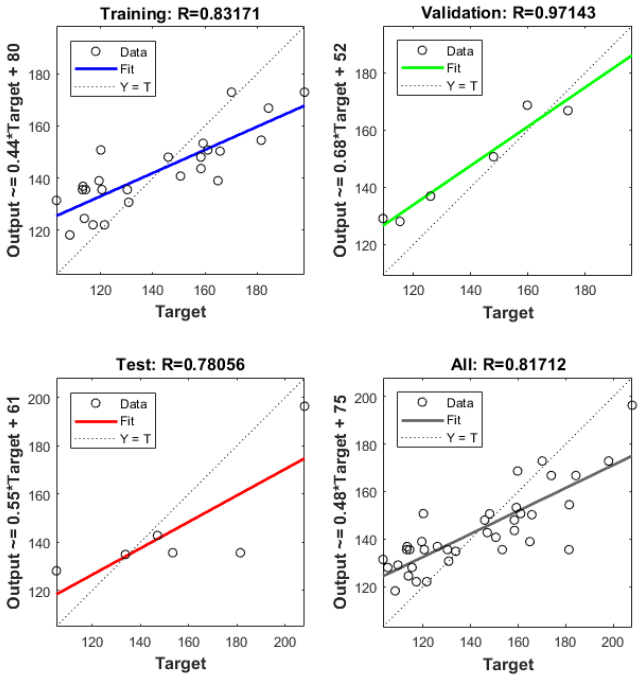

Fig. 5. Regression analysis of FF network

Fig. 6 shows the overall fit of RBF. It was found that the performance of the network worked based on the MSE was around 46 % better (an overall MSE performance of 164.78 $(MPa)^2$ was achieved). However, the RMSE performance difference is less and the actual RMSE of the RBF is around 12.84 MPa. The overall regression of the RBF achieves an accuracy of 88.95 %.

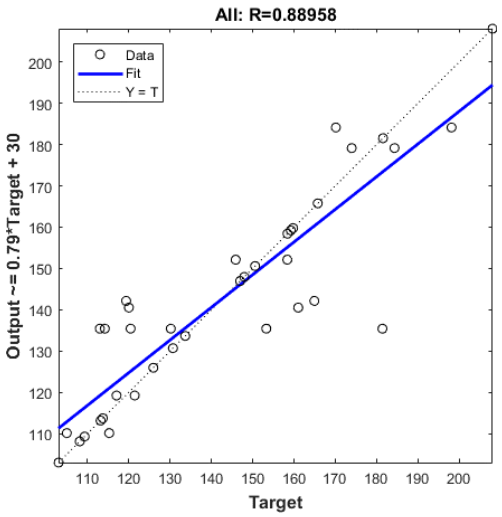

Fig. 6. Regression analysis of RBF network

The surface response model and regression analysis for the machining parameter on residual stress is shown in Fig. 7. This shows that feed rate has the most influential effect on the residual plane stress in the machining process followed by the cutting speed (surface speed), depth of cut and the tool lead angle. The feed rate has a quadratic function behavior, similar to the negative quadratic behavior in cutting speed and depth of cut. An increase of the feed rate also decreases the residual stress up to an optimum point, when the residual stress increases again.

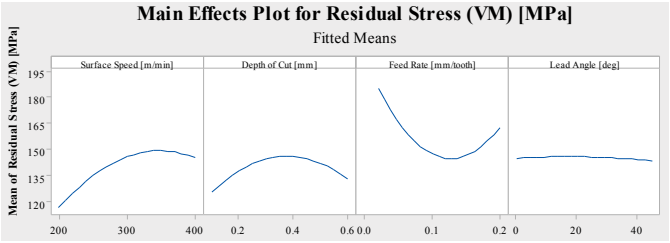

Fig. 7. Effect plot for experimental residual stress results

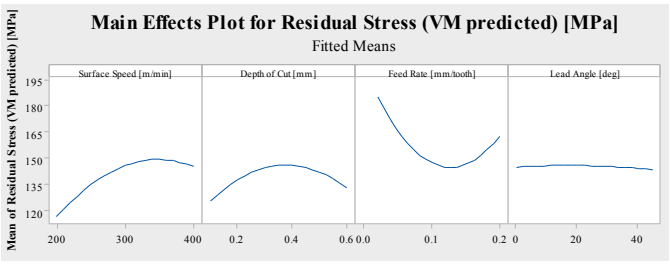

Fig. 8. Effect plot for predicted residual stress results

Fig. 8 shows the predicted results from the ANN, when using RBF. Comparing these results with the results from Fig. 7, it can be seen that they have a very good correlation.

5.2. Finite Element Model results

To develop an understanding for the evolvement of the residual stress during high speed milling a finite element simulation ran successfully. The simulation was compared with machining experiment No. 14 under the same machining parameters. The distribution of the plane residual stress based the JC formula is shown in Fig. 9. This illustration highlights that during cutting process, spikes of residual stress have developed on the cutting flute engagement and relaxation after the material removal.

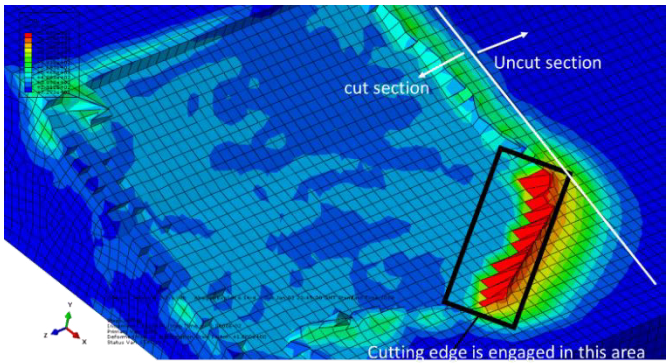

Fig. 9. Residual stress (VM) of experiment No.14 in FE model during cutting

Fig. 10 shows the top residual plane stress is 130.39 MPa in the FE simulation. The corresponding experiment has a plane stress of around 125.96±12 MPa, which is well within the measuring tolerances of the XRD.

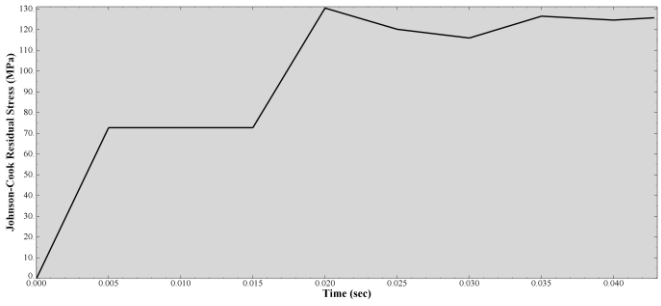

Fig. 10. VM residual stress vs. time in FE simulation

Heat is usually mainly responsible for generating tensile residual stress [17] in machining. The FE model shows the cutting temperatures does not exceed 420 °C. Such low temperatures illustrate that no work hardening has taken place during the cutting process (as shown in Fig. 11). The quick rising and cooling back to room temperature at the work piece leads to tensile stresses on the machined surface and sub-surfaces.

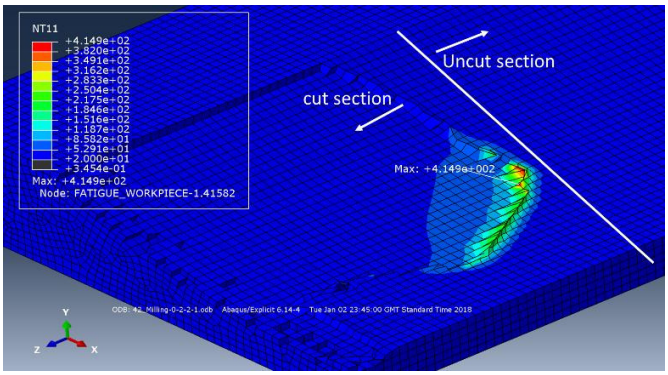

Fig. 11. Temperature distribution in work piece during cutting process

The above mentioned feed rate influences the residual stress the most, in form of a quadratic function, this is mainly due to the heat induction on the work piece. Applying a higher feed rate, heat on the deformed material increases and therefore the resistance of material removal decreases and less residual stresses occur in the work piece. However, if the feed rate is too high the relative motion between work piece and tool become faster than the material can be removed by the cutting tool. The heavily deformed and heated material remains on the work piece with a higher residual stress.

6. Conclusion

This work is a part of a research study to investigate and optimize high speed machining in a finishing process of a hard material. For analyzing and prediction of residual stress Artificial Neural Networks have been used. It was found that:

- The RBF model provides a more consistent and precise prediction for residual stress. This is due to the irregular response surface of the residual stress and small sample set.
- The feed rate was the most influencing factor on the plane residual stress state.
- During the machining process cutting temperature does not rise to more than 420 °C and therefore no work hardening of the material occurs. The adiabatic heating, which heats the work piece up in a very short time and let it cool immediately, encloses tensile stresses on the surface and subsurface, which was reflected by the experiment as well as the FE-Simulation.

Acknowledgements

The authors would like to acknowledge the financial and technical support from the Advanced Forming Research Centre (AFRC), UK and its machining team for this study.

References

[1] Axinte D,Dewes R. High-speed milling of AISI H13 hot-work tool steel using polycrystalline cubic boron nitride ball-nose mills: From experimental investigations and empirical modelling to functional testing of the machined surfaces. P I Mech Eng-B: J Eng 2010;2241: 15-24.
[2] Li W, Guo Y,Guo C. Superior surface integrity by sustainable dry hard milling and impact on fatigue. CIRP Ann-Manuf Techn 2013. 621: 567-570.
[3] Li W,Guo Y. Residual stress and fatigue properties of AISI H13 steel by sustainable dry milling. ASME 2012 International Manufacturing Science and Engineering Conference collocated with the 40th North American Manufacturing Research Conference and in participation with the International Conference on Tribology Materials and Processing. American Society of Mechanical Engineers 2012.
[4] Jawahir I, et al. Surface integrity in material removal processes: Recent advances. CIRP Ann-Manuf Techn 2011;. 602: 603-626.
[5] Umbrello D, et al. A hybrid finite element method–artificial neural network approach for predicting residual stresses and the optimal cutting conditions during hard turning of AISI 52100 bearing steel. Mater Design 2008;294: 873-883.
[6] Reimer A, Fitzpatrick S, Luo X.A full factorial numerical investigation and validation of precision end milling process for hardened tool steel, Euspen's 17th Internation Conference & Exhibition. Euspen: Hannover, Germany 2017.
[7] Reimer A, et al. Numerical Investigation of Mechanical Induced Stress during Precision End Milling Hardened Tool Steel. Solid State Phenomena. Trans Tech Publ. 2017.
[8] International A, Committee AIH,Committee AIAPD. Metals Handbook: Properties and selection: ASM international; 1990
[9] Shatla, M, Kerk, C,Altan, T, Process modeling in machining. Part I: determination of flow stress data. Int J Mach Tool Manu 2001;4110: 1511-1534.
[10] Xie T, Yu H,Wilamowski B. Comparison between traditional neural networks and radial basis function networks. Industrial Electronics (ISIE), IEEE International Symposium. IEEE. 2011;1194-9.
[11] Abdalla OA, et al. A comparison of feed-forward back-propagation and radial basis artificial neural networks: A Monte Carlo study. Information Technology (ITSim), 2010 International Symposium in. IEEE. 2010.
[12] Perez, C,Calderon JDD. Comparison Between Feed-Forward Back-Propagation and Radial Basis Functions Networks for Roughness Modeling in Face-Milling of Aluminum. ASME 2011 International Mechanical Engineering Congress and Exposition. American Society of Mechanical Engineers 2011.
[13] Outeiro, J. Surface integrity predictions and optimisation of machining conditions in the turning of AISI H13 tool steel. Int. J. Mach. and Machinability of Mat (IJMMM) 2014; 151-2: 122-134.
[14] Al Hazza MH, Adesta EY. Investigation of the effect of cutting speed on the Surface Roughness parameters in CNC End Milling using Artificial Neural Network. IOP Conference Series: Materials Science and Engineering. IOP Publishing 2013.
[15] An L, Liu S,Zhang H. Study on the Influence of Machining Parameters on Surface Residual Stresses in Dry Turning Inconel718 using FEA and ANN. Proceedings of the 9th International Conference on Computer and Automation Engineering. ACM 2017.
[16] Outeiro J. Optimization of Machining parameters for improved surface integrity of AISI H13 tool steel. 2012.
[17] Davim JP.Surface integrity in machining. Berlin: Springer; 2010